

# Transition from electrostatic-to-electromagnetic mode in a radio-frequency Ar inductively coupled plasma in atmospheric pressure

M. Abdur Razzak,<sup>a)</sup> Kenji Kondo, Yoshihiko Uesugi, Noriyasu Ohno, and Shuichi Takamura  
*Department of Energy Engineering and Science, Graduate School of Engineering, Nagoya University,  
Nagoya 464-8603, Japan*

(Received 23 May 2003; accepted 28 October 2003)

The dynamics of mode transition from the electrostatic ( $E$ ) to electromagnetic ( $H$ ) mode of a radio-frequency argon inductively coupled plasma (ICP) in atmospheric pressure is investigated, both experimentally and theoretically. High-speed (4500 f/s) camera imaging is performed to investigate the dynamics of  $E$ - $H$  discharge mode transition. The temporal plasma loading impedance of Ar inductive discharges at the  $E$ - $H$  transition stage is also observed to investigate the transition dynamics. The experimental observations reveal that the formation of the multiple streamerlike electrostatic discharge paths followed by the strong ring-shaped azimuthal discharges leads to ignite the high-pressure (around 1 atm or more) ICPs. The time scale of  $E$ - $H$  discharge mode transition is estimated by using proposed models and the estimated results are compared with that of the experimental one. It is found that the estimated results agree well with that of the experimental one. © 2004 American Institute of Physics. [DOI: 10.1063/1.1635650]

## I. INTRODUCTION

High-pressure radio-frequency (rf) inductive discharges have drawn considerable attention from a diverse group of researchers over the last few decades due to its wide range of operating conditions and various industrial and commercial applications.<sup>1-4</sup> However, so far, attention has been given to heating, sustainment, and stabilization of rf induction plasmas. But, when operated at high pressures (around 1 atm or more), initial startup is one of the most important issues to ignite the discharge of induction thermal plasmas, as the starting of high-pressure rf plasma torches are hard, and a high-voltage initiation is usually required.<sup>4</sup> So far, several techniques, such as dc arc jet<sup>5</sup> and low-pressure small-size plasma torch,<sup>6</sup> are used to initiate the high-pressure rf inductive discharges. But, these hybrid plasma torches characteristically operate at power levels of 50 to 100 kW or even more, where the dimensions of the second-stage high-power unit make it difficult to initiate and operate in a stable manner.<sup>4</sup> Therefore, the initiation of high-pressure rf inductive discharges with moderate rf power is an interesting and challenging issue, and with that in mind, we have investigated the high-pressure (1 atm) inductively coupled plasma (ICP) discharges at the ignition stage.

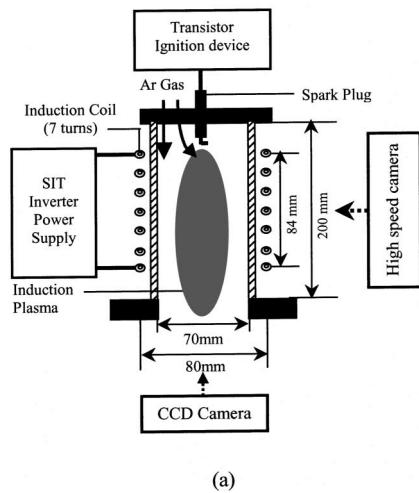
It has already been established that typical rf-generated plasmas are operated in two well-known modes: A capacitively coupled or electrostatic mode ( $E$  mode) and inductively coupled or electromagnetic mode ( $H$  mode). Recently, attention has been renewed to investigate the dynamics of this  $E$ - $H$  discharge mode transition and many theoretical and experimental works have been conducted, but mainly for very low-pressure (mTorr range) discharges,<sup>7-12</sup> because of the simple and easy generation, and diagnostics of low-pressure ICPs. The hysteresis and  $E$ - $H$  discharge mode tran-

sition in low pressure ( $\sim 150$  mTorr) ICPs have been reported by Kunje *et al.*<sup>7</sup> and Turner *et al.*,<sup>8</sup> taking the power balance argument and possible nonlinear mechanisms into account for sustaining the plasmas. Three-dimensional optical emission spectroscopy with computer tomography is used by Myoshi *et al.*<sup>9</sup> to explain the  $E$ - $H$  discharge mode transition in low-pressure ( $\sim 300$  mTorr) ICPs. The dynamics of mode transition in low-pressure (50 mTorr) low-frequency (460 kHz) Ar and N<sub>2</sub> ICPs are reported by Ostrikov *et al.*<sup>10</sup> by observing the plasma images using a charge coupled device (CCD) camera with a long exposure time (approximately 17 ms). The initial startup of high-pressure Ar inductive discharges is reported by Uesugi *et al.*,<sup>12</sup> by observing the plasmas using only the CCD camera, and also without explaining the physical mechanism and transition properties of  $E$ - $H$  discharge. However, by using the conventional CCD camera, it is very difficult to observe the  $E$ - $H$  discharge mode transition mechanism since the transition time is very short. Besides, in the papers mentioned above, the  $E$ - $H$  discharge mode transition time, which is very important factor for the generation of induction plasmas, is not estimated or modeled. Therefore, the motivation of this work is to investigate the time needed for the mode transition, and the transition properties together with the  $E$ - $H$  mode transition mechanism of atmospheric pressure Ar induction plasmas in a frequency range of 0.5–1.5 MHz with a moderate rf power of about 2–10 kW. The mode transition time is estimated by using proposed models in this constraint and the estimated results are compared with that of the experimental one.

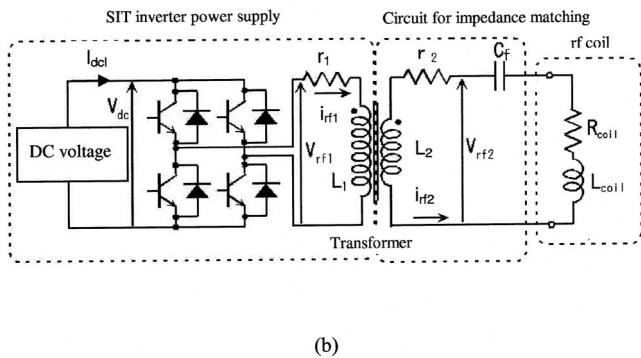
## II. EXPERIMENTS

The schematic diagram of experimental setup is depicted in Fig. 1(a). In the present experiment, a static induction transistor (SIT) inverter power source, the equivalent circuit of which is shown in Fig. 1(b), with a frequency range of

<sup>a)</sup>Electronic mail: razzak@ees.nagoya-u.ac.jp



(a)



(b)

FIG. 1. Schematic diagram of experimental setup.

0.2–2.0 MHz and a maximum output power of about 20 kW, is employed to generate Ar induction thermal plasmas in atmospheric pressure. An induction coil consisting of seven turns of a copper tube of 1/4 inch outer diameter is used as the loop antenna. The plasmas are sustained in a cylindrical Pyrex glass chamber with an internal diameter of 70 mm and length of 200 mm. Ar gas is injected both axially and swirly into the torch vessel with a total flow rate of 20–30 liter/min. The neutral gas pressure is controlled by using a mechanical rotary pump, and measured with a total pressure gauge. The rf power level, which is limited by the cooling capability of the system, is modulated with a 100 ms square wave pulse (extended up to 5 s). Repetitive spark discharge, using the spark discharge technique,<sup>12,14</sup> with a repetition frequency of 500 Hz and duration of 30 ms, is applied simultaneously with the rf pulse to initiate the discharge. This task is performed by using a simple automobile spark plug, placed at the center of the top flange of the vacuum chamber (shown in Fig. 1), with a high-voltage transformer circuit. A matching network is employed to optimize the plasma loading impedance and power coupling efficiency. A “FASTCAM-ultima SE” high-speed camera with a frame speed of 4500 f/s, located at the center of the discharge chamber and perpendicular to the discharge axis (shown in Fig. 1), is used to observe the *E–H* transition dynamics.

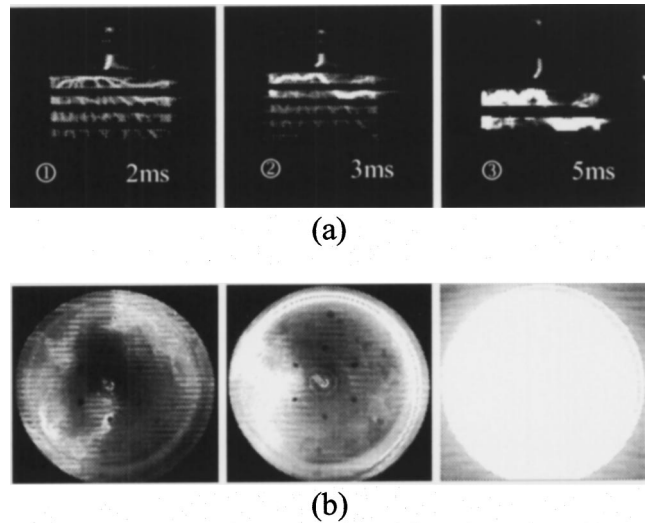


FIG. 2. Observation of mode transition dynamics by the high-speed camera imaging (a) and CCD camera imaging (b).

CCD camera imaging is also performed to investigate the discharge from the bottom by setting it beneath the torch vessel.

### III. ELECTROSTATIC-TO-ELECTROMAGNETIC TRANSITION DYNAMICS

The dynamics of *E–H* discharge mode transition observed by the high-speed camera imaging can briefly be described as follows: At the start of ignition, highly mobile electrons are accelerated and picked up energy from the applied electrostatic field,  $\tilde{E}_z$ , the average intensity of which is high enough (in the present experiment  $\sim 120$  kV/m) to excite and ionize the working gas thereby developing the multiple streamerlike discharge paths (*E* discharge) at the top of the torch chamber and very close to the inner surface of the discharge chamber [Figs. 2(a)① and 2(b)(left)] due to the stronger  $E_z$  near the torch surface. Then, the discharge paths connect among the streamers due to the induced electric field,  $\tilde{E}_\theta$  (in the present experiment  $\sim 2.5$  kV/m). But, the electron oscillating kinetic energy by these electric fields is not high enough to ionize the working gas. At this stage, collisional heating occurs due to the strong axial electrostatic field, which gives enough energy to the electrons. The induced azimuthal electric field promotes diffusive and/or convective drift motion for electrons in the azimuthal direction. These energetic electrons produce ionization and make electrically conducting bridges between neighboring streamers and transform the streamers into the ring-shaped azimuthal (*H*) discharge paths [Figs. 2(a)②,③ and 2(b)(middle)]. The conductive ring makes it possible to induce the azimuthal current and to inject the Joule power into the ring-shaped plasma. For the time being, the *H* discharge develops inward and downward thereby forming the steady-state plasmas [Fig. 2(b)(right)] due to Joule heating with the azimuthal rf current. From Fig. 2(b), it is seen that the discharges develop near the inner surface of the discharge vessel because of the stronger  $E_z$  and  $E_\theta$  near the torch surface than inside the chamber. From the experimental observation by fast camera

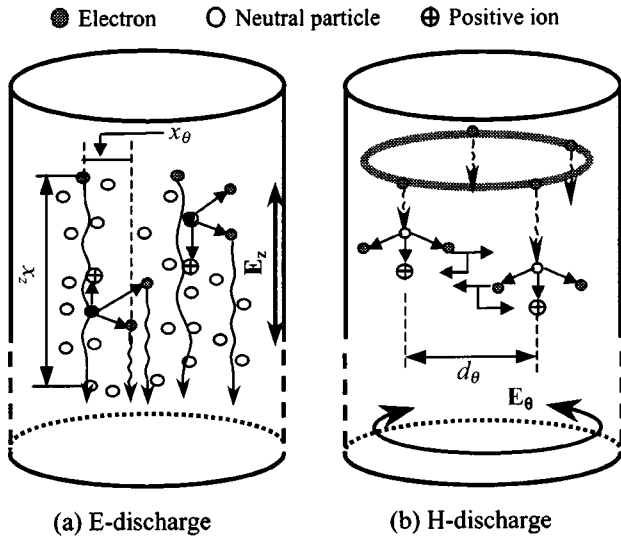


FIG. 3. Development of E and H discharge.

imaging, the E–H discharge mode transition time is found to be about 500–1000  $\mu\text{s}$ . This mode transition time can also be observed from the temporal plasma loading impedance, which will be described later in Sec. VI.

#### IV. ELECTROSTATIC–ELECTROMAGNETIC TRANSITION MODELING

##### A. Development of electrostatic discharge

Strong electrostatic field,  $E_z$  develops due to high rf power supply. Electrons are accelerated and collided with other gas molecules, especially with neutral particles, and gain energy from this applied electrostatic field to ionize neutral particles. The electrostatic field can be written as

$$\mathbf{E}_z = |E_z| e^{j(\omega t + \varphi)}, \quad (1)$$

where  $\omega$  is the driving angular frequency,  $\varphi$  is the initial phase of average electric field, and  $|E_z|$  is the amplitude of the electrostatic field, which is approximately given by

$$|E_z| = \frac{|V_{\text{coil}}|}{d} = \frac{\omega L_{\text{coil}} |I_{\text{rf}}|}{d}, \quad (2)$$

where  $L_{\text{coil}}$  is the inductance of the rf coil,  $|I_{\text{rf}}|$  is the amplitude rf coil current, and  $d$  is the vertical antenna length. We assume that the electron impact ionization is the dominant ionization process in the present condition, which is written as



The ionization mechanism can be described as follows: Initial electrons collide with the neutral particles and produce electron–ion pairs. The direction of motion of electrons depends on the polarity of the electrostatic field. The formed electrons, together with the primary electrons, repeat this processes and produce more free electrons. Therefore, cumulative ionizations can take place by the electrons along the direction of the electrostatic field to make streamers. The collision and ionization mechanisms are modeled as shown in Fig. 3(a).

Now, the electron kinetic energy is given by  $W = m_e |v_0|^2 / 2$ , where  $m_e$  is the electron mass and  $v_0$  is the electron oscillating velocity under the effects of  $E_z$  and electron–neutral collisions. The complex form of this oscillating velocity is given by

$$v_0 = \frac{e|E_z|}{m_e(j\omega + \nu_{en})} e^{j(\omega t + \varphi)}, \quad (4)$$

where  $e$  is the electronic charge, and  $\nu_{en}$  is the electron–neutral collision frequency. The typical value of  $\nu_{en}$  in the present condition is  $2.5 \times 10^{11}$  Hz, which is much higher than  $\omega$  ( $\sim 10^6$ ), so that Eq. (4) can be rewritten as

$$v_0 = \frac{e|E_z|}{m_e \nu_{en}} e^{j(\omega t + \varphi)}. \quad (5)$$

Therefore, the time-dependent heating power for an electron due to electron–neutral collision under the electrostatic field,  $E_z$  is given by

$$P(t) = e \text{Im}[v_0] \cdot \text{Im}[E_z]. \quad (6)$$

Using Eqs. (1) and (5), Eq. (6) can be rewritten as

$$P(t) = \frac{e^2 |E_z|^2}{m_e \nu_{en}} \sin^2(\omega t + \varphi). \quad (7)$$

As mentioned in Sec. III, the electron heating is necessary to reach the electron kinetic energy to the ionizing potential of Ar to have the ionization. This electron heating time can be calculated by using the power balance equation for electrons, which can be written as

$$\frac{dW(t)}{dt} = \frac{e^2 |E_z|^2}{m_e \nu_{en}} \sin^2(\omega t + \varphi) - \nu_{en} \frac{2m_e}{m_i} W(t), \quad (8)$$

where the first term on right-hand side of Eq. (8) represents the input power due to the electrostatic field,  $E_z$  and the second term represents the loss power due to electron–neutral elastic collision with the ion mass of  $m_i$ . Here, we neglect the loss due to the inelastic collision, because we are discussing the time scale when the electrons achieve the energy capable for ionization. Now, the analytical solution of Eq. (8) is

$$W(t) = L(1 - e^{-Mt}) - N\{2\omega \sin(2\omega t + 2\varphi) + M \cos(2\omega t + 2\varphi) - (2\omega \sin 2\varphi + M \cos 2\varphi)e^{-Mt}\}, \quad (9)$$

where

$$L = \frac{e^2 |E_z|^2 m_i}{4m_e^2 \nu_{en}^2}, \quad M = \frac{2m_e}{m_i} \nu_{en},$$

and

$$N = \frac{e^2 |E_z|^2}{2m_e \nu_{en} \left\{ \left( \frac{2m_e \nu_{en}}{m_i} \right)^2 + 4\omega^2 \right\}}.$$

However, each electron has its own phase  $\varphi$  so that we should take the average over  $\varphi$  for the electron cloud to rewrite Eq. (9) as

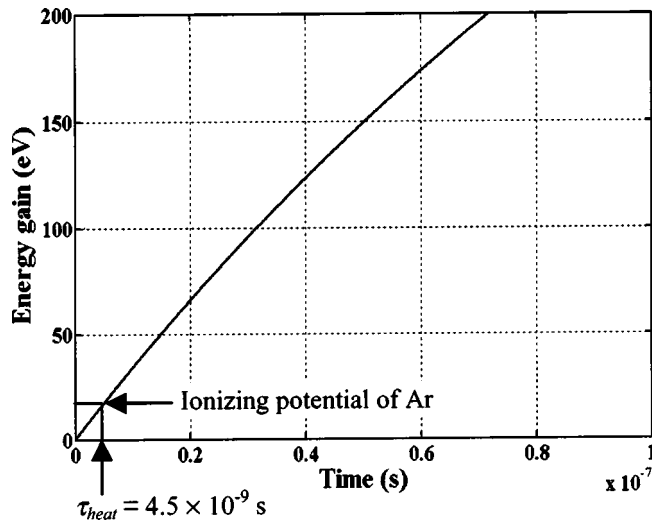


FIG. 4. Estimation for electron heating time from the development of electron kinetic energy in time.

$$\langle W(t) \rangle_{\varphi} = L(1 - e^{-Mt}) \approx LMt. \quad (10)$$

Therefore, the approximate value of electron heating time,  $\tau_{\text{heat}}$  to have single ionization, that is, to reach the electron kinetic energy to the ionizing potential of Ar, can be estimated from Eq. (10) as

$$\tau_{\text{heat}} = \frac{e\Phi_i}{LM} = \frac{2m_e v_{en} \Phi_i}{e|E_z|^2}, \quad (11)$$

where  $\Phi_i$  is the ionizing potential of Ar. The electron heating time versus electron energy gain is plotted in Fig. 4 and we should focus only on the initial phase of this figure. Under the present conditions ( $f = 1$  MHz and  $p = 100$  kPa), the typical average value of electron heating time is estimated  $4.5 \times 10^{-9}$  s, which is very much shorter than that of the rf period ( $\sim 10^{-6}$  s). Since the ionization time estimated by the ionization cross section ( $10^{-11}$  s in the present condition) is much shorter than the electron heating time ( $4.5 \times 10^{-9}$  s), the ionization starts as soon as the electron energy reaches the ionizing potential of Ar and, therefore, multiple thin streamerlike discharge paths develop in the axial direction, which is called the electrostatic discharge or  $E$  discharge as shown in Fig. 2(a), due to the cumulative ionizations by the strong electrostatic field,  $E_z$ .

Now, the drift displacement of an electron traveling during the electron heating time in the axial direction to have one ionization event can be written as

$$\lambda_z = \int_{\varphi}^{\varphi + \tau_{\text{heat}}} \frac{e|E_z|}{m_e v_{en}} \sin(\omega t + \varphi) dt. \quad (12)$$

The value of  $\lambda_z$  can be averaged over  $\varphi$  to rewrite Eq. (12) as

$$\bar{\lambda}_z = \sqrt{\langle \lambda_z^2 \rangle_{\varphi}} \approx \frac{e|E_z| \tau_{\text{heat}}}{\sqrt{2} m_e v_{en}}. \quad (13)$$

The typical value of  $\bar{\lambda}_z$  calculated from Eq. (13) is found to be 225  $\mu\text{m}$ .

## B. Transition from electrostatic-to-electromagnetic mode

The azimuthal electric field,  $E_{\theta}$ , is induced inside the discharge vessel due to the oscillating magnetic field produced by the applied coil current. The discharge paths connect among the streamers thereby forming ring-shaped discharges as shown in Fig. 3(b) due to this induced electric field in the azimuthal direction, which can be written as

$$E_{\theta} = \frac{|\epsilon|}{l} = \frac{\left| -\frac{d\Phi}{dt} \right|}{2\pi r} = \frac{d}{dt} \int \mathbf{B} \cdot d\mathbf{S}. \quad (14)$$

With  $d/dt = i\omega$ ,

$$|E_{\theta}| = \frac{\omega \int \mathbf{B} \cdot d\mathbf{S}}{2\pi r} = \frac{B_z \omega \pi r^2}{2\pi r} = \frac{B_z \omega r}{2}. \quad (15)$$

Applying Ampere's circuital law, Eq. (15) can be rewritten as

$$|E_{\theta}| = \omega \mu_0 r H_z / 2 = \mu_0 \omega r n I_{\text{rf}} / 2, \quad (16)$$

where  $r$  is the radius of torch of inner surface,  $n$  is the number of antenna turns per meter, and  $I_{\text{rf}}$  is the rf coil current.

The connection mechanism between neighboring streamers [shown in Fig. 3(b)] can be described as follows: The formed electrons, which gain sufficient energy from the applied electrostatic field,  $E_z$  to ionize other neutral particles, move slightly in the azimuthal direction. The direction of rf electric field which these formed electron face may be the same as or opposite to that of the old electrons since the phase is a random number between 0 and  $2\pi$ . Therefore, the probability of moving these electrons may be in either direction, clockwise, or counterclockwise depending on the phase and the direction of the alternating azimuthal electric field,  $E_{\theta}$ . The movement of these formed electrons can be treated as stochastic due to the random collisions with the neutral particles. These electrons, together with the primary electrons, repeat this process and produce more free electrons, which move diffusively in the azimuthal direction. This process continues until the electrically conducting bridge between neighboring streamers has been formed. Therefore, we may define this phenomenon as the collisional diffusion process, and under this condition, the characteristic time to connect between two neighboring streamers can be written as

$$\tau_c = \frac{d_{\theta}^2}{2D}, \quad (17)$$

where  $d_{\theta}$  is the typical distance between two neighboring streamers in  $\theta$  direction (2.5 mm in the present condition) and  $D$  is the diffusion coefficient, which can be expressed by

$$D = \frac{\Lambda^2}{2\tau}, \quad (18)$$

where  $\Lambda$  is the characteristic diffusion length and  $\tau$  is the characteristic diffusion time. Using Eq. (18), Eq. (17) can be rewritten as

$$\tau_c = \left( \frac{d_{\theta}}{\Lambda} \right)^2 \tau. \quad (19)$$

Equation (19) is considered to be the characteristic time needed for the  $E-H$  discharge mode transition. In this equation, the most important thing is to define the characteristics diffusion time,  $\tau$  and the characteristic diffusion length,  $\Lambda$ . In the present operating condition, we found the electron heating time for a cascading birth of electrons ( $4.5 \times 10^{-9}$  s) is much longer than the so-called electron impact ionization time ( $\sim 10^{-11}$  s) and the electron-neutral collision time ( $\sim 10^{-12}$  s). Therefore, we may choose the electron heating time,  $\tau_{\text{heat}}$  as the characteristics diffusion time,  $\tau$ . On the other hand, the azimuthal position of formed electrons, either clockwise or counterclockwise with respect to the original position of old electrons, depends on the phase of the azimuthal rf electric field as described in Sec. IV A. Therefore, we may choose the characteristic diffusion length,  $\Lambda$  as the drift displacement of the electron which traveled during the electron heating time in the azimuthal direction to have one ionization event, which can be written as

$$\lambda_{\theta} = \int_{\varphi}^{\varphi + \tau_{\text{heat}}} \frac{e|E_{\theta}|}{m_e \nu_{en}} \sin(\omega t + \varphi) dt. \quad (20)$$

The value of  $\lambda_{\theta}$  can be averaged over  $\varphi$  to rewrite Eq. (20) as

$$\bar{\lambda}_{\theta} = \sqrt{\langle \lambda_{\theta}^2 \rangle_{\varphi}} \approx \frac{e|E_{\theta}| \tau_{\text{heat}}}{\sqrt{2} m_e \nu_{en}}. \quad (21)$$

The typical value of  $\bar{\lambda}_{\theta}$  estimated from Eq. (21) is found 5.6  $\mu\text{m}$ . Using Eqs. (11) and (21), the first candidate of the time needed for the  $E-H$  mode transition can be found from Eq. (19) as

$$\tau_{c1} = \left( \frac{d_{\theta}}{\lambda_{\theta}} \right)^2 \tau_{\text{heat}} = \frac{m_e \nu_{en} |E_z|^2 d_{\theta}^2}{e \Phi_i |E_{\theta}|^2}. \quad (22)$$

On the other hand, during the half cycle of rf field, many electrons have been formed in the azimuthal direction due to multiple ionizations. This process continues until the electrically conducting bridge between neighboring streamers occurs. Under this condition, we may choose the characteristic diffusion time,  $\tau$  as the rf period,  $T$ , and the characteristic diffusion length,  $\Lambda$  as the mean excursion length,  $x_{\theta}$  in the azimuthal direction during the half cycle of the rf period, which can be written as

$$x_{\theta} = \int_0^{T/2} \frac{e|E_{\theta}|}{m_e \nu_{en}} \sin(\omega t + \varphi) dt. \quad (23)$$

The value of  $x_{\theta}$  can be averaged over  $\varphi$  to rewrite Eq. (23) as

TABLE I. Typical parameters for  $E-H$  transition modeling.

Plasma parameter	Value
Electron-neutral collision frequency, $\nu_{en}$	$2.5 \times 10^{11}$ (Hz)
Electron-impact ionization frequency, $\nu_{en}^i$ (with electron energy of 20 eV)	$10^{11}$ (Hz)
Electron heating time for single ionization, $\tau_{\text{heat}}$	$4.5 \times 10^{-9}$ (s)

$$\bar{x}_{\theta} = \sqrt{\langle x_{\theta}^2 \rangle_{\varphi}} \approx \frac{\sqrt{2}}{\pi} \frac{e|E_{\theta}|}{m_e \omega \nu_{en}}. \quad (24)$$

Therefore, using Eqs. (11) and (24), the second candidate of the time needed for the  $E-H$  mode transition can be found from Eq. (19) as

$$\tau_{c2} = \left( \frac{d_{\theta}}{x_{\theta}} \right)^2 T = \frac{\omega \pi^3 m_e^2 \nu_{en}^2 d_{\theta}^2}{e^2 |E_{\theta}|^2}. \quad (25)$$

Finally, during the half cycle, the induced electric field can be considered as dc because a half period  $T/2$  is quite long compared with the time needed for one ionization event. We assume that such an ionized plasma is convected with the effective electron kinetic energy  $W_{\theta} = 1/2 m_e v_{\theta}^2$ . Under this condition, the third candidate of the characteristic time needed for  $E-H$  mode transition can be written as

$$\tau_{c3} = \frac{d_{\theta}}{c_s}, \quad (26)$$

where  $c_s$  is the effective ion sound velocity due to ambipolar drift and is given by

$$c_s = \sqrt{\frac{W_{\theta}}{m_i}} = \frac{1}{\sqrt{2}} \sqrt{\frac{m_e}{m_i}} v_{\theta}, \quad (27)$$

with  $v_{\theta}$  as the oscillating velocity due to the induced electric field,  $E_{\theta}$  and is given by

$$v_{\theta} = \frac{e|E_{\theta}|}{m_e \nu_{en}} e^{j(\omega t + \varphi)}. \quad (28)$$

Using Eq. (27), the time needed for the  $E-H$  mode transition can be found from Eq. (26) as

$$\tau_{c3} = \frac{d_{\theta}}{v_{\theta}} \sqrt{\frac{2m_i}{m_e}}. \quad (29)$$

### V. COMPARISON BETWEEN ESTIMATED AND EXPERIMENTAL RESULTS

According to our proposed models described in the previous section, Eqs. (22), (25), or (29) can be considered as

TABLE II. Typical discharge parameters for  $E$  and  $H$  mode.

Discharge parameter	E mode	H mode
Oscillating velocity, $v_z$ and $v_{\theta}$	$70 \times 10^3$ (m/s)	$1.75 \times 10^3$ (m/s)
Electric field, $E_z$ and $E_{\theta}$	$100 \times 10^3$ (V/m)	$2.5 \times 10^3$ (V/m)
Mean excursion length, $x_z$ and $x_{\theta}$	$5 \times 10^{-3}$ (m)	$125 \times 10^{-6}$ (m)
Drift displacement of electron, $\lambda_z$ and $\lambda_{\theta}$	$225 \times 10^{-6}$ (m)	$5.6 \times 10^{-6}$ (m)

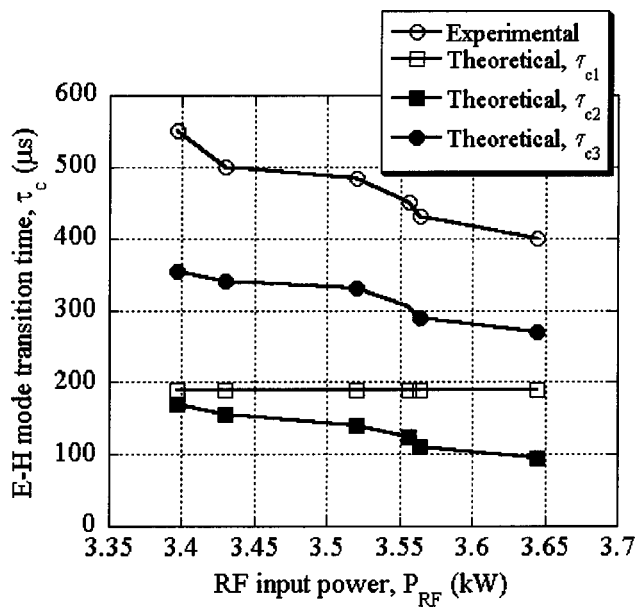


FIG. 5. rf power dependence of mode transition time (comparison between experimental and theoretical results at a fixed pressure of 20 kPa).

the time scale ( $\tau_c$ ) needed for the  $E-H$  discharge mode transition. The typical discharge parameters in the present operating conditions (atmospheric pressure Ar plasma with 1 MHz driving frequency) are shown in Tables I and II. The typical values of  $\tau_c$  calculated by Eqs. (22), (25), and (29) are found to be 900  $\mu s$ , 400  $\mu s$ , and 550  $\mu s$ , respectively, which are in the same order of magnitude.

On the other hand, from the experimental observation by fast camera imaging described in Sec. II, the  $E-H$  discharge mode transition time is found to be about 500–1000  $\mu s$ . Therefore, the  $E-H$  discharge mode transition times estimated from our proposed model (400–900  $\mu s$ ) agree well with that of the experimental result (500–1000  $\mu s$ ). However, at the moment, we are not sure about the process, which is dominant among these three candidates. The first two models are based on the diffusive motion of electrons while the last one is based on the convective ambipolar drift motion of electrons in the azimuthal electric field, which may have the highest possibility in the present condition. For better judgment, we may compare the dependence of rf power on the mode transition time estimated from Eqs. (22), (25), and (29) with those from the experimental observations by keeping the pressure fixed at 20 kPa, as shown in Fig. 5. It is noticed that the mode transition time decreases with increasing the rf input power, and the mode transition time calculated from the last model [Eq. (29)] is in good agreement with that of the experimental one than the other two approaches. Therefore, the last approach is considered to be the most convincing one.

## VI. PLASMA LOADING IMPEDANCE

Since the plasma heating mechanism is essential for high-pressure induction plasmas and the plasma resistance is the crucial quantity for heating mechanism and power coupling in induction plasma,<sup>13</sup> we measure the temporal plasma loading impedance at the transition stage, as depicted in Fig.

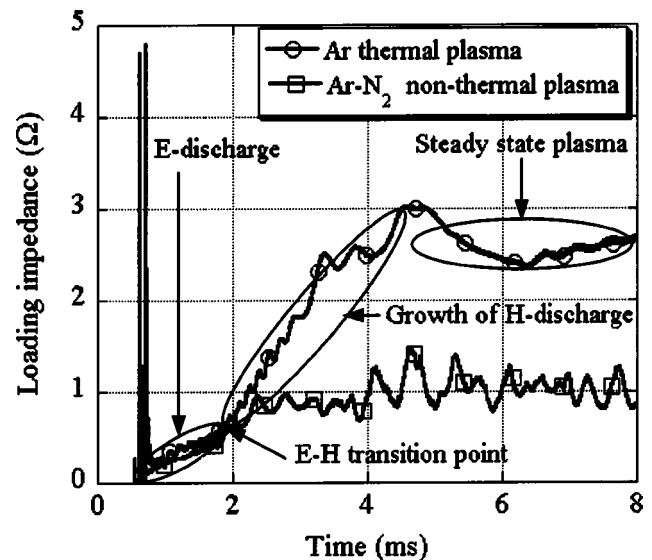


FIG. 6. Temporal plasma loading impedance of Ar induction plasma at atmospheric pressure.

6 to investigate the dynamics of the  $E-H$  discharge mode transition. The loading impedance was obtained by the ratio of voltage to current of the dc power supply of the SIT inverter circuit, as shown in Fig. 1(b). For the definition of rf plasma loading impedance, the readers are referred to Ref. 14. The development of the  $E$  discharge,  $E-H$  mode transition, development of  $H$  discharge and, finally, the formation of steady-state thermal plasmas can be seen clearly from the dynamic plasma loading impedance since the slope of the curve changes at every mode as shown in Fig. 6. It is noticed that the plasma loading impedance (or power absorbed by the plasma) at the start of ignition, i.e., in the  $E$ -discharge region is not high enough for plasma heating. But, the increment of loading impedance changes remarkably after the  $E-H$  mode transition, i.e., in the region of the development of the  $H$  discharge.

The gross  $E-H$  mode transition time, which is determined by various factors, such as ionization, Joule heating, loss mechanisms, etc., is found to be about 500–1000  $\mu s$ . In the present experiment, the vacuum impedance, i.e., the loading impedance without plasma, the loading impedance of  $E$  and  $H$  discharge of atmospheric pressure Ar induction plasma are found to be about 0.15, 0.15–0.25, and 0.25–3.0 ohm, respectively.

It can also be mentioned from Fig. 6 that no growth of loading impedance will be found if there is no development of the  $H$  discharge in the case of Ar- $N_2$  plasma, because the  $H$  discharge failed to be maintained due to an imbalance between the input energy gain and the strong radiative and/or convective energy loss due to high enthalpy nitrogen gas content. This will be discussed in another paper.

## VII. CONCLUSIONS

In this article, the temporal development of atmospheric pressure rf (0.5–1.5 MHz) Ar inductive discharges at the  $E-H$  mode transition stage and its transition properties, together with the transition mechanism, are investigated ex-

perimentally and analytically. From our experimental investigation, it is noticed that, in atmospheric pressure rf inductive discharges, first, the multiple streamerlike discharges are developed axially in the  $E$  mode and then, the streamers are transformed into the strong ring-shaped azimuthal discharges in the  $H$  mode to develop the steady-state induction thermal plasmas. It is also found that, unlike the low pressure ICPs,<sup>7–11</sup> high-pressure rf inductive discharges start to develop from the inner surface of the torch vessel as shown in Fig. 2(b) due to the stronger induced electric field near the torch surface. From the experiment, it is also clear that the  $E$ – $H$  discharge mode transition dynamics can also be observed from the behavior of the plasma loading impedance.

In this article, we also presented a plasma model with three different proposals to estimate the time scale of the  $E$ – $H$  discharge mode transition and compared the estimated results with that of the experimental one. It is found that the estimated transition times using the proposed models (400–900  $\mu$ s) agree well with that of the experimental result (500–1000  $\mu$ s).

#### ACKNOWLEDGMENTS

The authors would like to express their sincere gratitude for the cooperation of the program committee of NIFS (Na-

tional Institute for Fusion Science), Japan in providing the FASTCAM-ultima SE camera during the experiments.

- <sup>1</sup>M. I. Boulos, P. Fauchais, and E. Pfender, *Thermal Plasmas-Volume 1: Fundamentals and Applications* (Plenum, New York, 1994).
- <sup>2</sup>K. C. Paul and T. Sakuta, *Elec. Power Sys. Research* **56**, 185 (2000).
- <sup>3</sup>S. Xu, K. N. Ostrikov, Y. Li, E. L. Tsakadze, and I. R. Jones, *Phys. Plasmas* **8**, 2549 (2001).
- <sup>4</sup>J. Reece Roth, *Industrial Plasma Engineering-Volume 1: Principles* (Institute of Physics Publishing, Bristol, 1995).
- <sup>5</sup>T. Uesugi, O. Nakamura, T. Yoshida, and K. Akashi, *J. Appl. Phys.* **64**, 3874 (1988).
- <sup>6</sup>T. Yoshida, T. Tani, H. Nishimura, and K. Akashi, *J. Appl. Phys.* **54**, 640 (1983).
- <sup>7</sup>G. Cunge, B. Crowley, D. Vender, and M. M. Turner, *Plasma Sources Sci. Technol.* **8**, 576 (1999).
- <sup>8</sup>M. M. Turner and M. A. Lieberman, *Plasma Sources Sci. Technol.* **8**, 313 (1999).
- <sup>9</sup>Y. Myoshi, Z. L. Petrovic, and T. Makabe, *IEEE Trans. Plasma Sci.* **30**, 130 (2002).
- <sup>10</sup>K. Ostrikov, E. Tsakadze, J. Ning, L. Jidong, R. Storer, and S. Xu, *IEEE Trans. Plasma Sci.* **30**, 128 (2002).
- <sup>11</sup>U. Kortshagen, N. D. Gibson, and J. E. Lawler, *J. Phys. D* **29**, 1224 (1996).
- <sup>12</sup>Y. Uesugi, T. Adachi, K. Kondo, and S. Takamura, *Trans. IEE Japan* **122-A**, 461 (2002) (in Japanese).
- <sup>13</sup>N. S. Yoon, B. C. Kim, J. G. Yang, and S. M. Hwang, *IEEE Trans. Plasma Sci.* **26**, 190 (1998).
- <sup>14</sup>M. A. Razzak, K. Kondo, Y. Uesugi, and S. Takamura, *Proceedings of the Annual Meeting of the Fundamentals and Materials Society of IEE Japan* (IEE Japan, Yokohama, 2002), p. 112.